Evolution of a vortex sheet between two superfluids

Tomi Ruokola

Low Temperature Laboratory, Helsinki University of Technology,

P.O. Box 2200, FIN-02015 HUT, Finland

(Dated: June 14, 2005)

Contents

I. Introduction 2

II. Equation of motion for the vortex sheet 3

A. Boundary integral formulation 3

B. Interface dynamics 5

III. Numerical simulation 10

A. Algorithm 10

B. Results 12

IV. Conclusions 15

References 16

I. INTRODUCTION

A vortex sheet is formed at the interface of two fluids flowing past each other. In 1871 Lord Kelvin predicted [1] that the vortex sheet becomes unstable if the relative velocity of the fluids exceeds a certain critical limit. Today this Kelvin–Helmholtz instability is a well-known phenomenon in fluid mechanics. For instance, simulations [2] show that during the instability the vortex sheet rolls up into a spiral which eventually collides with itself, resulting in a breakdown of the interface.

Recent experiments with superfluids [3] provide a new testing ground for this classical phenomenon. The experimetal setup consists of two superfluid phases (conventionally called A and B) of ^{3}He rotating on top of each other at different velocities. When one of the fluids is accelerated beyond a certain limit, an instability of the interface is observed. Volovik [4] has amended Kelvin's theory to take into account the specific properties of superfluids, and the critical velocities predicted by this new theory are in good agreement with the experiments. However, the lifetime of the instability – the time it takes from the initial perturbation to the breakdown of the interface – is observed to be less than a second, whereas analytical estimates can give lifetimes of several minutes at low temperatures [5].

The purpose of this work is to explore this discrepancy in more detail. Specifically, the

analytical calculations of a previous report [6], based on a linearized system, are now complemented by numerical simulations using the full nonlinear equations.

II. EQUATION OF MOTION FOR THE VORTEX SHEET

A. Boundary integral formulation

Consider a two-dimensional velocity field $\mathbf{u}(x, y) = (u, v)$. We can define a stream function ψ such that $\mathbf{u} = \nabla \times (\psi \hat{\mathbf{z}})$, or,

$$u = \partial_y \psi, \quad v = -\partial_x \psi \tag{1}$$

provided that $\partial_x \partial_y \psi = \partial_y \partial_x \psi$, i.e., $\partial_x u + \partial_y v = 0$, which is satisfied by incompressible flow. Then the vorticity, $\boldsymbol{\omega} = \omega \hat{\mathbf{z}} = \nabla \times \mathbf{u}$, can be expressed as

$$\omega = \partial_x v - \partial_y u = -\nabla^2 \psi \tag{2}$$

This Poisson equation can be solved as

$$\psi(\mathbf{r}) = \int G(\mathbf{r}, \mathbf{r}') \omega(\mathbf{r}') da' \tag{3}$$

if G satisfies $\nabla^2 G(\mathbf{r}, \mathbf{r}') = -\delta(\mathbf{r} - \mathbf{r}')$. In two-dimensional space (with no boundaries) such a G is given by

$$G(\mathbf{r}, \mathbf{r}') = \frac{1}{2\pi} \ln \frac{1}{|\mathbf{r} - \mathbf{r}'|} = -\frac{1}{4\pi} \ln[(x - x')^2 + (y - y')^2] \tag{4}$$

because $\nabla^2 G(\mathbf{r}, \mathbf{r}') = 0$ for $\mathbf{r} \neq \mathbf{r}'$, and integrating over a disc centered at $\mathbf{r}$ yields

$$\int_D \nabla^2 G da' = \int_{\partial D} \frac{\partial G}{\partial n} ds' = -\frac{1}{2\pi} \int_0^{2\pi} \frac{1}{|\mathbf{r} - \mathbf{r}'|} |\mathbf{r} - \mathbf{r}'| d\theta = -1 \tag{5}$$

Now assume that the vorticity is concentrated on a strip of width ϵ around a curve C parametrized by arc length s. Then define the quantity γ as

$$\gamma(s) = \int_{-\epsilon/2}^{\epsilon/2} \omega(\mathbf{r}(s) + \hat{\mathbf{n}} l) dl \tag{6}$$

where $\hat{\mathbf{n}}$ is a unit normal to C at s. By taking the limit $\epsilon \to 0$, we arrive at the concept of vortex sheet strength γ. To characterize this quantity, let us return to the case of finite ϵ and integrate over a rectangle B (Fig. 1):

$$\int_{s_0}^{s_1} \gamma(s) ds = \int_B (\nabla \times \mathbf{u}) \cdot \hat{\mathbf{z}} da = \int_{\partial B} \mathbf{u} \cdot d\mathbf{l} \xrightarrow{\epsilon \to 0} \int_{s_0}^{s_1} (\mathbf{v}_1 - \mathbf{v}_2) \cdot \hat{\mathbf{s}} ds \tag{7}$$

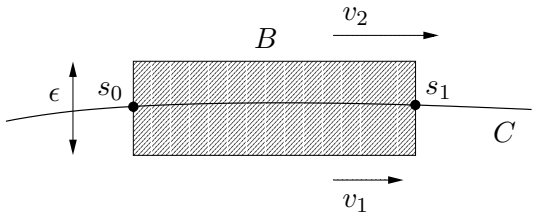

FIG. 1: We assume that all vorticity of the flow is concentrated on a strip of width ϵ around the interface curve C.

where the second equality follows from Stokes' theorem, and where $\hat{\mathbf{s}}$ is the unit tangent to C and $\mathbf{v}_i$ are the limiting velocities when approaching the vortex sheet from either side. In the limit $s_1 \to s_0$, Eq. (7) shows us that

$$\gamma = (\mathbf{v}_1 - \mathbf{v}_2) \cdot \hat{\mathbf{s}} \tag{8}$$

that is, the vortex sheet strength is equal to the jump in the tangential velocity across the boundary.

Eqs. (3), (4) and (6) can now be combined to give the stream function in the presence of a vortex sheet as

$$\psi = -\frac{1}{4\pi} \int \gamma(s) \ln[(x - x(s))^2 + (y - y(s))^2] ds \tag{9}$$

and the corresponding velocity components as

$$\begin{aligned} u &= -\frac{1}{2\pi} \int \gamma(s) \frac{y - y(s)}{(x - x(s))^2 + (y - y(s))^2} ds \\ v &= \frac{1}{2\pi} \int \gamma(s) \frac{x - x(s)}{(x - x(s))^2 + (y - y(s))^2} ds \end{aligned} \tag{10}$$

The following equations are most conveniently derived using complex analysis, and we therefore introduce the complex velocity $q = u + iv$ and position $z = x + iy$. Assume then that the vortex sheet is infinite and 1-periodic in the x direction. More precisely, take a new curve parameter α such that $x(\alpha+1) = x(\alpha)+1$ for all α. Then the periodicity requirement can be stated as $y(\alpha + 1) = y(\alpha)$, $\gamma(\alpha + 1) = \gamma(\alpha)$. Now, using Eq. (10), we can write q^*, the complex conjugate of q, as

$$q^* = u - iv = \frac{1}{2\pi i} \int_{-\infty}^{\infty} \frac{\tilde{\gamma}(\alpha)}{z - z(\alpha)} d\alpha = \frac{1}{2\pi i} \int_0^1 \tilde{\gamma}(\alpha) \sum_{n=-\infty}^{\infty} \frac{1}{z - z(\alpha) - n} d\alpha \tag{11}$$

where $\tilde{\gamma}(\alpha) = \gamma(\alpha)s_\alpha$ is an unnormalized vortex sheet strength; it is not equal to the velocity difference since its value also depends explicitly on the parametrization of the sheet. With the identity [7]:

$$\cot(z) = \sum_{n=-\infty}^{\infty} \frac{1}{z - n\pi} \tag{12}$$

Eq. (11) can be summed in closed form as

$$q^* = \frac{1}{2i} \int_0^1 \tilde{\gamma}(\alpha) \cot \pi(z - z(\alpha)) d\alpha \tag{13}$$

We have not yet specified the asymptotic behaviour of q. To this end, we note that

$$\cot(x + iy) = \frac{\sin 2x - i \sinh 2y}{\cosh 2y - \cos 2x} \to \mp i, \quad \text{as } y \to \pm\infty \tag{14}$$

and thus,

$$q^* \to \mp \tfrac{1}{2} \bar{\gamma} \tag{15}$$

where $\bar{\gamma}$ is the average of γ over the period. Therefore, if we wish to have the asymptotic velocities below and above the interface as $V_1\hat{\mathbf{x}}$ and $V_2\hat{\mathbf{x}}$, instead of Eq. (13) we must use

$$q^* = \frac{1}{2i} \int_0^1 \tilde{\gamma}(\alpha) \cot \pi(z - z(\alpha)) d\alpha + \bar{V} \tag{16}$$

where $\bar{V} = \frac{1}{2}(V_1 + V_2)$ and $\tilde{\gamma}$ is such that $\bar{\gamma} = V_1 - V_2$. The motion of the vortex sheet between two ordinary fluids depends only on their relative velocity, and in that case we could choose $\bar{V} = 0$. However, with superfluids also the velocity with respect to the container wall becomes significant (see next section, especially Eq. (44)).

Eq. (16) can then be used to find the velocity field anywhere within the fluid. To proceed further, we need to determine the time evolution of $\tilde{\gamma}(\alpha)$ and $z(\alpha)$.

B. Interface dynamics

For inviscid and incompressible flow, the Euler equation can be written as

$$\partial_t \mathbf{u} + \mathbf{u} \cdot \nabla \mathbf{u} = -\nabla\big(\frac{p}{\rho} + \varphi\big) \tag{17}$$

where ρ is the density, p the pressure, and φ an external potential. Since the flow is irrotational outside the vortex sheet, we can introduce the velocity potential ϕ such that $\mathbf{u} = \nabla\phi$.

Now we can write Eq. (17), on either side of the sheet, in the form of a Bernoulli equation

$$\partial_t \phi_1 + \tfrac{1}{2} v_1^2 + \frac{p_1}{\rho_1} + \varphi_1 = C_1(t) \tag{18}$$

$$\partial_t \phi_2 + \tfrac{1}{2} v_2^2 + \frac{p_2}{\rho_2} + \varphi_2 = C_2(t) \tag{19}$$

where $C_i(t)$ are arbitrary time-dependent integration constants. Taking the sum and difference of Eqs. (18) and (19), and denoting $\Delta p = p_1 - p_2$, gives

$$\partial_t(\phi_1 + \phi_2) + \tfrac{1}{2}(v_1^2 + v_2^2) + p_1 \frac{\rho_1 + \rho_2}{\rho_1 \rho_2} - \frac{\Delta p}{\rho_2} + \varphi_1 + \varphi_2 = C_1 + C_2 \tag{20}$$

$$\partial_t(\phi_1 - \phi_2) + \tfrac{1}{2}(v_1^2 - v_2^2) - p_1 \frac{\rho_1 - \rho_2}{\rho_1 \rho_2} + \frac{\Delta p}{\rho_2} + \varphi_1 - \varphi_2 = C_1 - C_2 \tag{21}$$

Eliminating p_1 from Eqs. (20) and (21) and taking the derivative with respect to the curve parameter α gives

$$\partial_\alpha \left\{ \partial_t(\phi_1 - \phi_2) + \tfrac{1}{2}(v_1^2 - v_2^2) + \varphi_1 - \varphi_2 + 2\frac{\Delta p}{\rho_1 + \rho_2} + A\Big[\partial_t(\phi_1 + \phi_2) + \tfrac{1}{2}(v_1^2 + v_2^2) + \varphi_1 + \varphi_2\Big] \right\} = 0 \tag{22}$$

where $A \equiv (\rho_1 - \rho_2)/(\rho_1 + \rho_2)$ is known as the Atwood number.

The kinematic boundary condition requires that the normal component of the fluid velocity is continuous across the interface, that is,

$$(\mathbf{v}_1 - \mathbf{v}_2) \cdot \hat{\mathbf{n}} = 0 \tag{23}$$

This, together with Eq. (8), implies

$$\mathbf{v}_1 \;=\; \mathbf{w} + \tfrac{1}{2}\gamma \hat{\mathbf{s}} \tag{24}$$

$$\mathbf{v}_2 \;=\; \mathbf{w} - \tfrac{1}{2}\gamma \hat{\mathbf{s}} \tag{25}$$

where $\mathbf{w} \equiv \frac{1}{2}(\mathbf{v}_1 + \mathbf{v}_2)$ is the average of the velocities on either side of the sheet.

To evaluate the derivatives of the form $\partial_\alpha \partial_t \phi$ in Eq. (22), we note that the functions $\partial_t \phi$ are given in Eulerian coordinates (x, y), i.e., in the frame of an outside observer. However, the derivative is taken with respect to the Lagrangian coordinate α, moving along with the vortex sheet. To derive the appropriate transformation, denote the Eulerian coordinate of the interface point α at time t as $\mathbf{r}$, that is, $\mathbf{r} = (x(\alpha, t), y(\alpha, t))$, and correspondingly for

time t' and the same α, $\mathbf{r}' = (x(\alpha, t'), y(\alpha, t'))$. Then we write for an arbitrary function g:

$$\begin{aligned}\frac{g(\mathbf{r}', t') - g(\mathbf{r}, t)}{t' - t} &\longrightarrow \frac{\partial g}{\partial t}\Big|_{\alpha} \\ &= \frac{g(\mathbf{r}', t') - g(\mathbf{r}', t)}{t' - t} + \frac{g(\mathbf{r}', t) - g(\mathbf{r}, t)}{\mathbf{r}' - \mathbf{r}} \cdot \frac{\mathbf{r}' - \mathbf{r}}{t' - t} \\ &\longrightarrow \frac{\partial g}{\partial t}\Big|_{x,y} + (\nabla g) \cdot \frac{\partial \mathbf{r}}{\partial t}\end{aligned} \tag{26}$$

that is,

$$\frac{\partial}{\partial t}\Big|_{x,y} = \frac{\partial}{\partial t}\Big|_{\alpha} - \tilde{\mathbf{w}} \cdot \nabla \tag{27}$$

where $\tilde{\mathbf{w}}(\alpha) \equiv \frac{\partial \mathbf{r}}{\partial t}$ is the velocity of the interface element at a fixed α. With the help of Eq. (27) we have

$$\begin{aligned}\partial_\alpha \big[\partial_t(\phi_1 - \phi_2)|_{x,y}\big] &= \partial_\alpha \big[\partial_t(\phi_1 - \phi_2)|_{\alpha}\big] - \tilde{\mathbf{w}} \cdot \nabla(\phi_1 - \phi_2) \\ &= \partial_t \big[\nabla(\phi_1 - \phi_2) \cdot \hat{\mathbf{s}} \partial_\alpha s\big] - \gamma \tilde{\mathbf{w}} \cdot \hat{\mathbf{s}} \\ &= \partial_t(\gamma \partial_\alpha s) - \gamma \tilde{\mathbf{w}} \cdot \hat{\mathbf{s}}\end{aligned} \tag{28}$$

and

$$\begin{aligned}\partial_\alpha \big[\partial_t(\phi_1 + \phi_2)|_{x,y}\big] &= \partial_\alpha \big[\partial_t(\phi_1 + \phi_2)|_{\alpha}\big] - \tilde{\mathbf{w}} \cdot \nabla(\phi_1 + \phi_2) \\ &= \partial_t \big[2\mathbf{w} \cdot \hat{\mathbf{s}} \partial_\alpha s\big] - 2\tilde{\mathbf{w}} \cdot \mathbf{w} \\ &= 2\partial_t \mathbf{w} \cdot \hat{\mathbf{s}} \partial_\alpha s + 2\mathbf{w} \cdot \partial_\alpha \tilde{\mathbf{w}} - 2\tilde{\mathbf{w}} \cdot \mathbf{w}\end{aligned} \tag{29}$$

where we have used $\partial_t(\hat{\mathbf{s}} \partial_\alpha s) = \partial_\alpha \partial_t \mathbf{r} = \partial_\alpha \tilde{\mathbf{w}}$ in the last equality.

Inserting Eqs. (24), (25), (28) and (29) into Eq. (22) gives an evolution equation for the vortex sheet strength γ:

$$\begin{aligned}&\partial_t(\gamma \partial_\alpha s) - \partial_\alpha[\gamma(\tilde{\mathbf{w}} - \mathbf{w}) \cdot \hat{\mathbf{s}}] + \partial_\alpha(\Delta p)/\bar{\rho} + \partial_\alpha(\varphi_1 - \varphi_2) = \\ &\qquad - 2A\Big[\partial_t \mathbf{w} \cdot \hat{\mathbf{s}} \partial_\alpha s - (\tilde{\mathbf{w}} - \mathbf{w}) \cdot \partial_\alpha \mathbf{w} + \tfrac{1}{8}\partial_\alpha \gamma^2 + \tfrac{1}{2}\partial_\alpha(\varphi_1 + \varphi_2)\Big]\end{aligned} \tag{30}$$

where $\bar{\rho} = (\rho_1 + \rho_2)/2$.

Because the position of the interface is defined by the position of the adjoining fluid elements, the boundary condition (23) requires that the normal components of the fluid and interface velocities are equal, or, in other words, $\tilde{\mathbf{w}} \cdot \hat{\mathbf{n}} = \mathbf{w} \cdot \hat{\mathbf{n}}$. However, the tangential component of the velocity of an interface element, $\tilde{\mathbf{w}} \cdot \hat{\mathbf{s}}$, is not determined by any physical consideration and can be chosen for computational convenience; we make the simplest choice of $\tilde{\mathbf{w}} = \mathbf{w}$, that is, the vortex sheet velocity is the average of the fluid velocities. Furthermore,

we assume that the fluids have equal densities, $\rho_1 = \rho_2 = \rho$, so that $A = 0$. Eq. (30) is then greatly simplified to

$$\partial_t \tilde{\gamma} = -\partial_\alpha \Big[\frac{\Delta p}{\rho} + \Delta\varphi \Big] \tag{31}$$

with $\Delta\varphi = \varphi_1 - \varphi_2$. The motion of the vortex sheet is now, at least in priciple, determined by Eqs. (16) and (31). But how do we calculate $\mathbf{w} = \frac{1}{2}(\mathbf{v}_1 + \mathbf{v}_2)$ from Eq. (16)? Denoting by q_1, q_2 and w the complex counterparts of $\mathbf{v}_1$, $\mathbf{v}_2$ and $\mathbf{w}$, the so-called Sokhotski–Plemelj formulas state that [8]

$$q_1^*(\alpha) = \frac{1}{2i}\,\mathrm{P}\!\int_0^1 \tilde{\gamma}(\alpha') \cot \pi(z(\alpha) - z(\alpha'))d\alpha' - \tfrac{1}{2}\tilde{\gamma}(\alpha)\partial_\alpha s + \bar{V} \tag{32}$$

$$q_2^*(\alpha) = \frac{1}{2i}\,\mathrm{P}\!\int_0^1 \tilde{\gamma}(\alpha') \cot \pi(z(\alpha) - z(\alpha'))d\alpha' + \tfrac{1}{2}\tilde{\gamma}(\alpha)\partial_\alpha s + \bar{V} \tag{33}$$

and therefore

$$w^*(\alpha) = \tfrac{1}{2}(q_1^* + q_2^*) = \frac{1}{2i}\,\mathrm{P}\!\int_0^1 \tilde{\gamma}(\alpha') \cot \pi(z(\alpha) - z(\alpha'))d\alpha' + \bar{V} \tag{34}$$

where P denotes the Cauchy principal value. This singular integral, known as the Birkhoff–Rott equation [9], can now be used to calculate the velocity of the vortex sheet. Since computing the principal value is somewhat inconvenient, we can use the identity [10]

$$\mathrm{P}\!\int_0^1 \cot \pi(z(\alpha) - z(\alpha'))\partial_\alpha z(\alpha')d\alpha' = 0 \tag{35}$$

to regularize the integral in Eq. (34); multiply Eq. (35) by $\tilde{\gamma}(\alpha)/2i\partial_\alpha z(\alpha)$ and subtract it from Eq. (34). The result is

$$w^*(\alpha) = \frac{1}{2i}\int_0^1 \frac{\tilde{\gamma}(\alpha')\partial_\alpha z(\alpha) - \tilde{\gamma}(\alpha)\partial_\alpha z(\alpha')}{\partial_\alpha z(\alpha)} \cot \pi(z(\alpha) - z(\alpha'))d\alpha' + \bar{V} \tag{36}$$

which is non-singular. This is the equation we use in the simulation for the motion of the vortex sheet.

Before any practical calculation, we must still specify the physics behind the force terms $\Delta p/\rho$ and $\Delta\varphi$ in Eq. (31). In this work we assume that Δp is produced by two forces, one due to surface tension σ and other due to damping Γ:

$$-\Delta p ds = df_\sigma + df_\Gamma \tag{37}$$

By definition, the surface tension σ is equal to the energy expended when a surface element ds is stretched by an amount δs, that is, $\delta E = \sigma\delta s$. Now take the situation depicted in

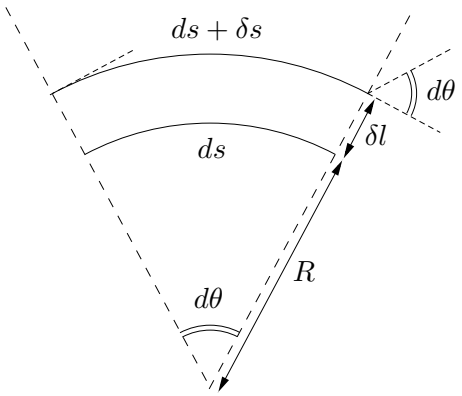

FIG. 2: Geometry of an infinitesimal curve segment.

Fig. 2: element ds, short enough to be considered an arc of a circle of radius R, is stretched by displacing it in the normal direction by δl. Since $ds/R = (ds + \delta s)/(R + \delta l)$, we have

$$\delta s = \kappa \delta l ds \tag{38}$$

where $\kappa \equiv 1/R$ is the curvature of s at ds. With this notation, the force exerted on the interface element can be written as

$$df_\sigma = \frac{\delta E}{\delta l} = \kappa \sigma ds \tag{39}$$

To derive an analytic expression for κ, we note that $ds = Rd\theta$, where $d\theta$ is the change in the tangent angle over ds. Therefore

$$\kappa = \frac{d\theta}{ds} = \frac{\partial_\alpha \theta}{\partial_\alpha s} = \frac{\partial_\alpha \theta}{[(\partial_\alpha x)^2 + (\partial_\alpha y)^2]^{1/2}} \tag{40}$$

Because $\tan\theta = \frac{dy}{dx}$, we have

$$\frac{d\tan\theta}{d\alpha} = (1 + \tan^2\theta)\partial_\alpha \theta = \frac{\partial_\alpha x \partial_\alpha^2 y - \partial_\alpha y \partial_\alpha^2 x}{(\partial_\alpha x)^2} \tag{41}$$

which can be solved for $\partial_\alpha \theta$ as

$$\partial_\alpha \theta = \frac{1}{1 + \tan^2\theta} \frac{\partial_\alpha x \partial_\alpha^2 y - \partial_\alpha y \partial_\alpha^2 x}{(\partial_\alpha x)^2} = \frac{\partial_\alpha x \partial_\alpha^2 y - \partial_\alpha y \partial_\alpha^2 x}{(\partial_\alpha x)^2 + (\partial_\alpha y)^2} \tag{42}$$

Combining Eqs. (40) and (42) gives the curvature as

$$\kappa = \frac{\partial_\alpha x \partial_\alpha^2 y - \partial_\alpha y \partial_\alpha^2 x}{[(\partial_\alpha x)^2 + (\partial_\alpha y)^2]^{3/2}} \tag{43}$$

Even with nonviscous fluids, the motion of the interface can still be damped, and this is indeed the case for the interface between the A and B phases of superfluid ^{3}He [11]. The damping force is proportional to the normal velocity of the interface, that is,

$$df_\Gamma = -\Gamma \hat{\mathbf{n}} \cdot \mathbf{w} ds \tag{44}$$

Finally, the bulk forces are assumed to be due to a magnetic field $\mathbf{H}$, so that the potential difference over the interface is

$$\Delta\varphi = \tfrac{1}{2}(\chi_2 - \chi_1)|\mathbf{H}|^2/\rho \tag{45}$$

where χ_i are the magnetic susceptibilities of the two fluids. We further assume that the field does not depend on the x coordinate, i.e., $\mathbf{H} = H\hat{\mathbf{y}}$, and approximate

$$\tfrac{1}{2}H^2 = \tfrac{1}{2}H_0^2 + yH_0\partial_y H \tag{46}$$

where H_0 and $\partial_y H$ are the magnetic field and its gradient at $y = 0$. Then, combining Eqs. (31), (37), (39), (44), (45) and (46) yields

$$\partial_t \tilde{\gamma} = \partial_\alpha \Big[\frac{\sigma}{\rho}\kappa - \frac{\Gamma}{\rho}\hat{\mathbf{n}} \cdot \mathbf{w} - \frac{\Delta\chi H_0 \partial_y H}{\rho} y \Big] \tag{47}$$

where $\Delta\chi = \chi_2 - \chi_1$ and κ is given by Eq. (43). Now, Eqs. (36) and (47) are the complete equations of motion for the variables $x(\alpha)$, $y(\alpha)$ and $\tilde{\gamma}(\alpha)$.

III. NUMERICAL SIMULATION

A. Algorithm

Based on the formulation of the preceding section, we have implemented a simple time integration algorithm by discretizing x, y and $\tilde{\gamma}$ in space and time. First, the variables are discretized evenly in the parameter α, with the following dimensionless initial values:

$$\begin{aligned} x(\alpha) &= \alpha \\ y(\alpha) &= 0.01\ \sin(2\pi\alpha) \\ \tilde{\gamma}(\alpha) &= 1 \end{aligned} \tag{48}$$

so that the unit of velocity is $\bar{\gamma} = V_1 - V_2$, where V_i are the time-independent asymptotic velocities, as defined above Eq. (16). The unit of length is the width of the computational

region, L. In the experiment [3], one of the fluids is stationary in the container frame, and we therefore choose $V_2 = 0$, which implies $\bar{\gamma} = V_1 \equiv v$ and $\bar{V} = \frac{1}{2}v$ (or $\bar{V} = \frac{1}{2}$ in dimensionless form) in Eq. (36). Because we are mostly interested in the behaviour of the system near the critical velocity, we choose L to be equal to the critical wavelength of the instability (see next section).

By introducing the Weber number We, the Richardson number Ri, and the parameter Γ' as

$$\begin{aligned} \mathrm{We} &= \frac{\rho v^2 L}{\sigma} \\ \mathrm{Ri} &= \frac{\Delta\chi H_0 \partial_y H L}{\rho v^2} \\ \Gamma' &= \frac{\Gamma}{\rho v} \end{aligned} \tag{49}$$

we can write Eq. (47) in dimensionless form:

$$\partial_t \tilde{\gamma} = \mathrm{We}^{-1} \partial_\alpha \kappa - \Gamma' \partial_\alpha (\hat{\mathbf{n}} \cdot \mathbf{w}) - \mathrm{Ri}\, \partial_\alpha y \tag{50}$$

Thus we see that there are three independent parameters in the simulation: We, Ri, and Γ'. However, in the experiment, the tunable parameters are the flow velocity v, pressure p, temperature T, and magnetic field gradient $\partial_y H$. Here we choose the values $p = 30$ bar, $T = 0.4\, T_c$ (T_c is the superfluid transition temperature), and $\partial_y H = 44$ T/m. Using standard references, for instance [12], then gives $\rho = 86.9$ kgm^{-3}, $\sigma = 2.29 \cdot 10^{-8}$ Jm^{-2}, $H_0 = 0.483$ T, and $\Delta\chi = 0.718$ JT^{-2}m^{-3}. With these values and Eq. (49) we can translate between numerical and experimental parameters.

To advance the simulation, the variables are integrated from timestep i to $i+1$ with the following algorithm (Δt is the length of the timestep and $\mathbf{r} = (x, y)$):

$$\begin{aligned} &\partial_t \mathbf{r}^i = \partial_t \mathbf{r}(\mathbf{r}^i, \tilde{\gamma}^i) \qquad \text{(from Eq. (36))} \\ &\partial_t \tilde{\gamma}^i = \partial_t \tilde{\gamma}(\mathbf{r}^i, \partial_t \mathbf{r}^i) \qquad \text{(from Eq. (50))} \\ &\textbf{repeat} \\ &\quad \mathbf{r}^{i+1} = \mathbf{r}^i + \partial_t \mathbf{r}^i \cdot \Delta t \\ &\quad \tilde{\gamma}^{i+1} = \tilde{\gamma}^i + \partial_t \tilde{\gamma}^i \cdot \Delta t \\ &\quad \partial_t \mathbf{r}^i = \partial_t \mathbf{r}(\mathbf{r}^{i+1}, \tilde{\gamma}^{i+1}) \\ &\quad \partial_t \tilde{\gamma}^i = \partial_t \tilde{\gamma}(\mathbf{r}^{i+1}, \partial_t \mathbf{r}^i) \\ &\textbf{until } \tilde{\gamma}^{\mathbf{i+1}} \textbf{ converges to a given tolerance} \end{aligned} \tag{51}$$

The integral in Eq. (36) is computed with the trapezoidal rule, and the derivatives in Eqs. (36) and (50) with central finite differences.

B. Results

In this section we compare the numerical simulations with the analytical calculations of a previous work [6]. These calculations show that the instability starts with the critical wave vector

$$k_0 = \sqrt{\frac{F}{\sigma}} \tag{52}$$

when the flow velocity v exceeds the value

$$v = \frac{(4F\sigma)^{1/4}}{\rho^{1/2}} \tag{53}$$

where $F = \Delta\chi H_0 \partial_y H$. The critical velocity for the instability is 3.69 mm/s when using the parameters given in the preceeding section. We choose to examine the flow with velocity $v = 4.00$ mm/s and periodicity $L = 2\pi/k_0 = 0.244$ mm.

We still have to fix a value for the damping constant Γ. Its dependence on p and T is not very well known, but a theory by Kopnin [11] gives an estimate

$$\Gamma = \frac{3.606\, m^{*2} k_B^3 T^3}{\pi^3 \hbar^3 \Delta_A} \ln\left(\frac{E_F}{T}\right) \tag{54}$$

where m^* is the effective mass, Δ_A the A phase gap, and E_F the Fermi energy. In our case Eq. (54) predicts the value $\Gamma = 0.019$ Jsm^{-4}, and this is what we shall use.

The results of the first simulation are plotted in Fig. 3a, which shows the time evolution of the wave height h, defined as $h(t) = \frac{1}{2}[y_{\max}(t) - y_{\min}(t)]$, where $y_{\max}(t) = \max_\alpha y(\alpha, t)$, and similarly for $y_{\min}(t)$. We notice that the number of grid points, N, has a marked effect on the result of the simulation. Using a very large number of points is not possible since we found out that using $N \gtrsim 1000$ makes the algorithm numerically unstable. Furthermore, on an average run, more that 99% of the computational time is spent evaluating the integral (36), where the number of steps scales as N^2, and hence, the total execution time also scales as N^2. Already at $N = 800$ computing the evolution of one second in Fig. 3a takes about 10^5 time steps, or 40 hours on a Pentium 4. Taking longer time steps is not feasible since this also makes the simulation unstable. We therefore try to extrapolate the results to the limit $N \to \infty$; in this limit we should recover the physically correct behaviour. The extrapolation

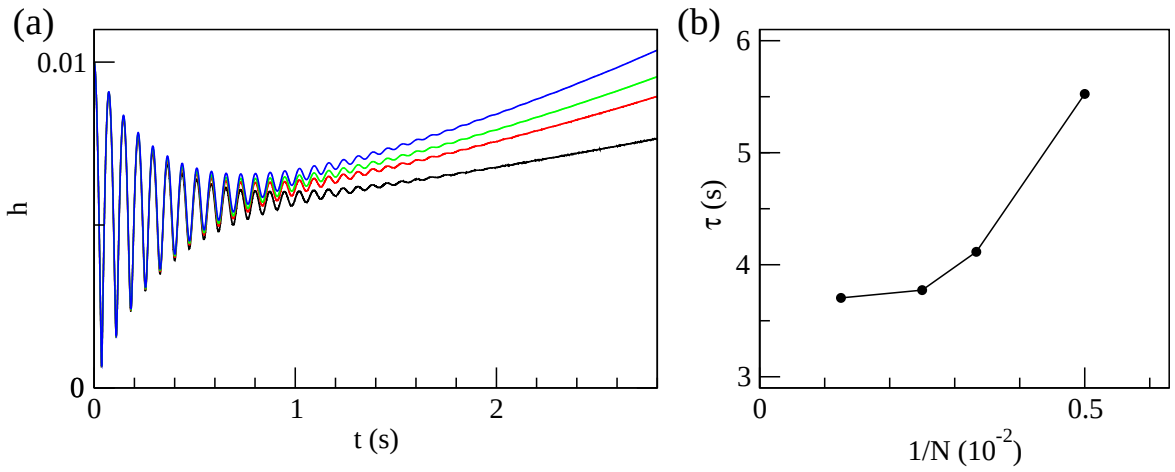

FIG. 3: (a) Time evolution of the height of the interfacial wave, h, with $v = 4.00$ mm/s and $\Gamma = 0.019$ Jsm^{-4}. The four curves show the results for different numbers of grid points N: $N = 200$ (bottom), $N = 300$, $N = 400$, and $N = 800$ (top). We have fitted an exponential function $h \sim \exp(t/\tau)$ to these curves, and figure (b) shows the dependence of the time constant τ on the inverse of N. We can estimate that as $N \to \infty$, τ tends to $\tau = 3.7$ s.

is accomplished by fitting an exponential curve $h \sim \exp(t/\tau)$ to the numerical results (in the initial oscillatory period we use the time average of $h(t)$ for fitting). Then, Fig. 3b shows that with increasing N, τ tends to $\tau = 3.7$ s. An analytical calculation with a linearized equation of motion shows that the instability should grow exponentially with a time constant $\tau = 3.65$ s, so the agreement with the numerical value is excellent.

The results of another run, with $v = 4.50$ mm/s and $\Gamma = 0.300$ Jsm^{-4}, are shown in Fig. 4. Since v and Γ are larger than in Fig. 3, the growth of the instability is significantly faster. In this case a single exponential curve, with $\tau = 0.11$ s, fits all three numerical results. Analytical calculations give $\tau = 0.107$ s, again a complete agreement.

Fig. 5 shows snapshots of the waveform from the same simulation as Fig. 4. We see that the amplitude grows tenfold while the shape is slightly deformed from the initial sinusoidal curve. However, the simulation becomes unstable at $t = 0.27$ s. The reason for the instability is apparently the clustering of the data points (Fig. 6). This clustering is made possible by the fact that the points are allowed to move freely in the x–y plane; they are not, for instance, fixed to stay equidistant from each other. Unfortunately, this instability cannot be avoided, at least in practice, by taking shorter timesteps because the required step is so short that the simulation effectively freezes.

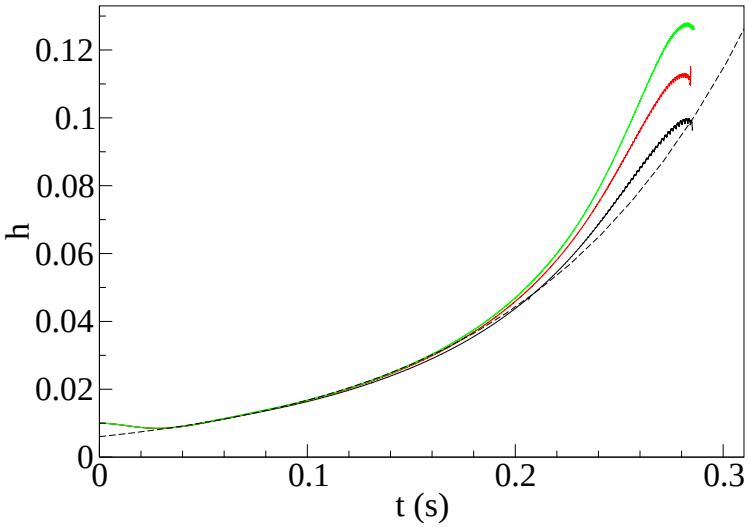

FIG. 4: Time evolution of the height of the interfacial wave, h, with $v = 4.50$ mm/s and $\Gamma = 0.300$ Jsm^{-4}. The three solid curves show the results for different numbers of grid points N: $N = 200$ (bottom), $N = 400$, and $N = 800$ (top). The dashed curve is an exponential function $h \sim \exp(t/\tau)$ with $\tau = 0.11$ s.

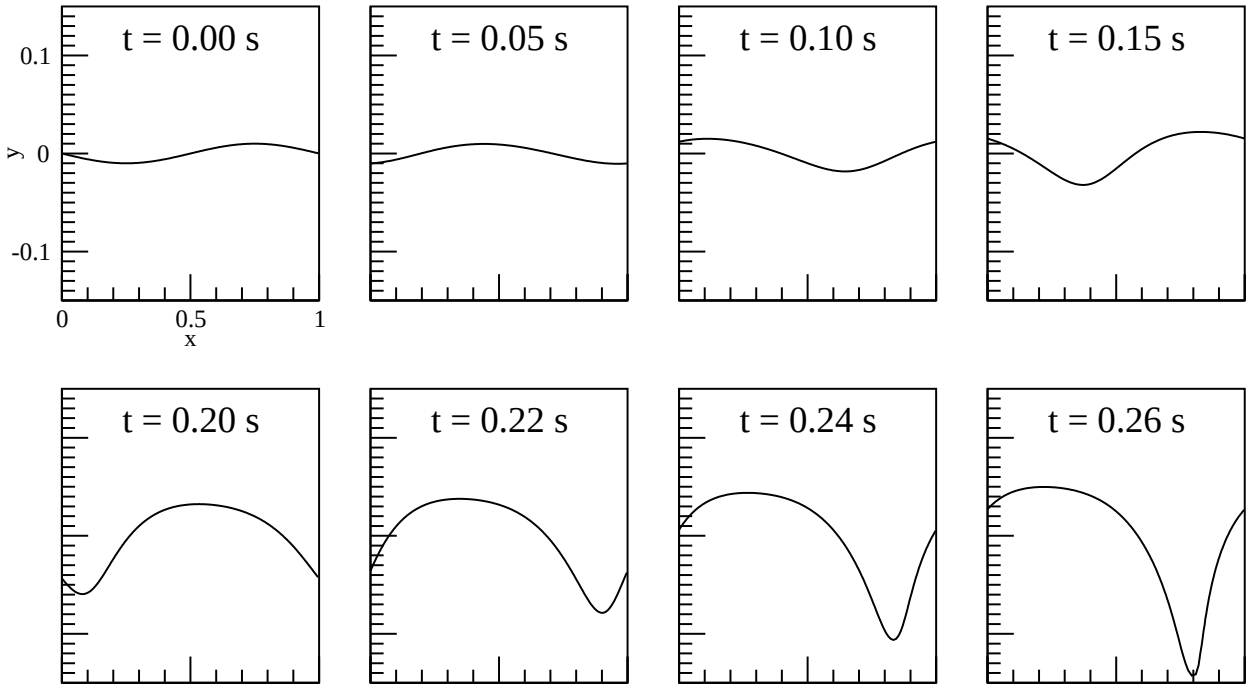

FIG. 5: An x–y plot of the waveform at different times with parameters $v = 4.50$ mm/s and $\Gamma = 0.300$ Jsm^{-4}, as in Fig. 4. The number of grid points used in the simulation is $N = 400$.

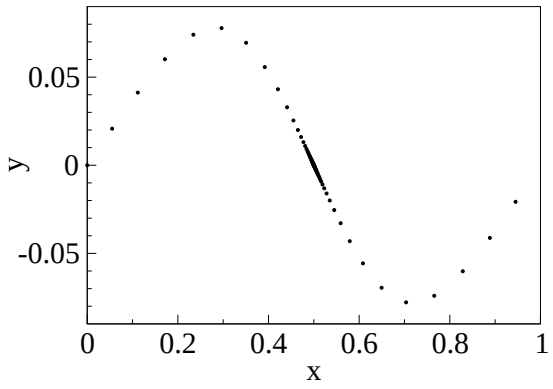

FIG. 6: An illustration of the clustering of the data points. In this simulation we have a total of $N = 80$ points, but about 50 of them are densely gathered on one short curve segment. This results in a loss of accuracy and eventually a numerical instability sets in.

IV. CONCLUSIONS

We have numerically investigated the time evolution of the Kelvin–Helmholtz instability of a vortex sheet between two superfluid phases. The KH instability has been intensively studied in the literature but, to our knowledge, this is the first simulation where the interfacial damping between the two fluids is taken into account.

We have found that the numerical results are in good agreement with earlier analytical calculations. More specifically, as can be seen from Fig. 4, the amplitude follows extremely closely the analytically predicted exponential curve $\exp(t/\tau)$ until $t \approx 1.5\tau$. During $t \approx 1.5\tau \ldots 2.5\tau$ we can see some nonlinear behaviour: the wave is deformed from the sinusoidal shape (Fig. 5) and it grows super-exponentially. However, for $t > 2.5\tau$ we have no data due to the numerical instability of the algorithm. Most likely this instability is due to the clustering of data points; this problem has also been identified, and solved, by other authors [2]. A future project is to make our algorithm more robust so that we can simulate the evolution of the sheet well into the nonlinear regime. It is clear that the wave cannot grow indefinitely; at some point it must break down, but we do not know when and how this happens.

Our primary goal was to investigate the discrepancy between theory and experiment concerning the instability lifetime. The simulations confirm the analytical estimates: close to the critical velocity the wave grows for several seconds before breakdown, not a fraction of

a second as is experimentally observed. The main suspect is the damping parameter Γ: if Γ were considerably larger than predicted by Eq. (54), this problem would be solved. In fact, other experiments [13] also suggest that the theoretical value of Γ is about 2 orders of magnitude too small. This means that the physics of the ^{3}He AB phase boundary requires some reconsideration.

---

[1] Lord Kelvin, *Mathematical and physical papers*, vol. 4 (Cambridge University Press, 1910).

[2] T. Y. Hou, J. S. Louwengrub, and M. J. Shelley, Phys. Fluids **9**, 1933 (1997).

[3] R. Blaauwgeers, V. B. Eltsov, G. Eska, A. P. Finne, R. P. Haley, M. Krusius, J. J. Ruohio, L. Skrbek, and G. E. Volovik, Phys. Rev. Lett. **89**, 155301 (2002).

[4] G. E. Volovik, JETP Lett. **75**, 418 (2002).

[5] G. E. Volovik, JETP Lett. **76**, 240 (2002).

[6] T. Ruokola (2004), special assignment.

[7] I. S. Gradshteyn and I. M. Ryzhik, *Table of Integrals, Series, and Products* (Academic Press, 2000), 6th ed.

[8] N. I. Muskhelishvili, *Singular Integral Equations* (Noordhoff, Groningen, 1953).

[9] G. Birkhoff, in *Hydrodynamic Instability*, edited by G. Birkhoff, R. Bellman, and C. Lin (American Mathematical Society, 1962), vol. XIII of *Proc. Symp. Appl. Math.*, p. 55.

[10] G. R. Baker, D. I. Meiron, and S. A. Orszag, J. Fluid Mech. **123**, 477 (1982).

[11] N. B. Kopnin, Sov. Phys.–JETP **65**, 1187 (1987).

[12] W. P. Halperin and E. Varoquaux, in *Helium three*, edited by W. P. Halperin and L. P. Pitaevskii (North-Holland, Amsterdam, 1990).

[13] M. Bartkowiak, S. N. Fisher, A. M. Guénault, R. P. Haley, G. N. Plenderleith, G. R. Pickett, and P. Skyba, Physica B **284**, 240 (2000).